

Full Length Research Paper

Simulation-based microwave imaging of plain and reinforced concrete for nondestructive evaluation

Oguz Gunes^{1*} and Oral Buyukozturk²

¹Department of Civil Engineering, Cankaya University, Ankara, Turkey.

²Department of Civil and Environmental Engineering, Massachusetts Institute of Technology, Cambridge, MA, USA.

Accepted 13 December, 2011

The focus of this paper is the implementation of a backpropagation algorithm as a potential solution for the inverse source problem for microwave imaging of plain and reinforced concrete targets. The data used in imaging was obtained from numerical simulation of far-field microwave scattering by concrete targets using typical frequency bandwidth of commercially available radar systems. A finite difference-time domain (FD-TD) technique was used for the simulations. Electromagnetic (EM) properties of concrete for various moisture conditions were obtained from a previous study. A total of four simulations were performed using a Gaussian pulse wave excitation for dry and moisture saturated concrete cylinders with and without a rebar at the center. The reflected and transmitted fields were recorded along two measurement lines. Images reconstructed using the backpropagation algorithm showed the potential of the method for concrete non destructive testing (NDT) while drawing attention to its limitations mainly due to the linearizing assumptions made in the algorithm's formulation.

Key words: Nondestructive testing (NDT), microwave, imaging, concrete, ground penetrating radar (GPR), finite difference-time domain (FD-TD), simulation, backpropagation.

INTRODUCTION

Imaging of concrete structures for nondestructive testing purposes can be defined in a broad sense as obtaining a representation of certain physical properties of the concrete material and characteristics of the physical system using techniques that will not damage the structure or permanently impair its serviceability (Buyukozturk, 1998; Yu and Buyukozturk, 2009; Buyukozturk and Yu, 2009). Imaging concrete is a challenging task since concrete is a highly non-homogeneous material. It is generally produced in the field with limited quality control. Grain size distribution is highly variable and the properties of the constituent materials are greatly varied making it difficult to obtain accurate images. Other sources of difficulties in imaging concrete structures include the generally complex physical geometry, existence of inclusions, restricted accessibility of the object and the problems related to the

sensitivity of the imaging method to the inhomogeneities in concrete.

The method of using microwaves, more widely known as the ground penetrating radar (GPR), for nondestructive testing of concrete involves generating and transmitting short electromagnetic (EM) pulses or time harmonic waves through a transmitter antenna towards a target medium and recording the scattered signals at the receiver antenna. When the incident EM waves encounter an object or another medium with different EM properties, some portion of the transmitted energy is reflected from the boundary and the rest is transferred into the new medium undergoing some refraction depending on the material properties of the new medium and the angle of incidence. Figure 1 illustrates the reflected, refracted and transmitted waves originated from the encounter of an incident wave with a scatterer. These waves are collectively called the scattered waves. The scattered signals recorded at the receiver contain some information about the target's EM properties which can be extracted by processing and interpreting the recorded signals.

*Corresponding author. E-mail: ogunes@alum.mit.edu. Tel: +90 312 233 1406.

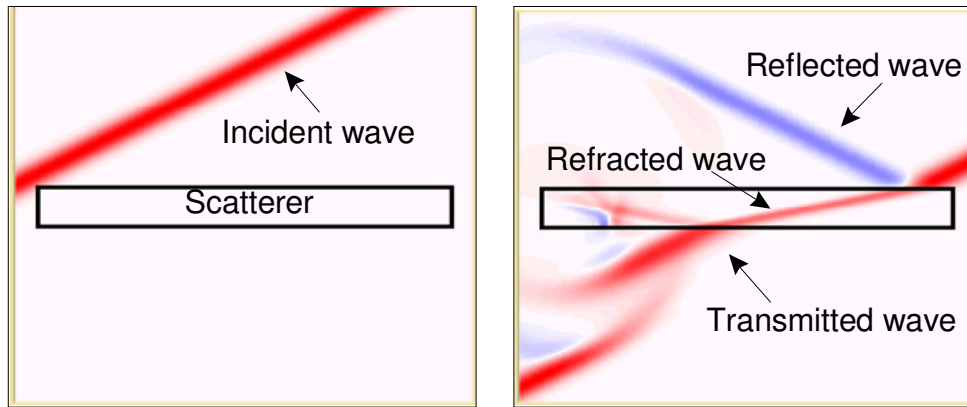


Figure 1. Reflection, refraction and transmission of an incident electromagnetic wave propagating through an object.

Microwave imaging involves reconstruction of the target's representation in terms of its EM properties using the scattered fields either in transmission or reflection mode, obtained by illuminating the object from many directions or along a synthetic aperture. This is generally achieved through appropriate inversion methods which are referred to as inverse scattering methods or identification methods (Herman et al., 1987; Boerner, 1983; Bertero and Pike, 1992). Image reconstruction can be performed using either iterative algorithms or transform-based algorithms (Kak and Slaney, 1988). The main shortcoming of iterative algorithms is that they do not consider diffraction which can be defined as the interference effects giving rise to illumination beyond the geometrical shadow (Cartz, 1995). Diffraction becomes important when the dimensions of the inhomogeneities are comparable to the wavelength of the radiation which is generally the case for microwave non destructive testing (NDT) of concrete. Transform-based methods involve processing of the scattered data partially or completely in the Fourier domain depending on the algorithm. After coherently superposing multi-frequency and/or multidimensional measurement data, the object is reconstructed by an inverse Fourier transform. The advantage of transform-based algorithms is that diffraction effects can be taken into consideration. Possible disadvantages include large computation and memory requirements, difficulty in incorporating a priori information into reconstruction, and the requirement for linearizing approximations (Kak and Slaney, 1988).

ELECTROMAGNETIC PROPERTIES OF CONCRETE

Application of microwave imaging to concrete structures requires an in depth understanding of the EM properties of concrete and how these properties affect its interaction with the EM waves. Various aspects of EM wave

scattering such as the amount of reflection from the concrete target, the velocity and wavelength of waves inside concrete, and the degree of attenuation are all related to the material properties. The significance of the EM properties of concrete in this research was that the data used in imaging studies was obtained from numerical simulation of EM wave scattering which requires the EM properties of concrete as input parameters. Unfortunately, the knowledge available on EM properties of concrete is very limited compared to the amount of information available on its mechanical properties. So far, very few research studies have been conducted investigating the EM properties of hardened concrete. In this research, modeling of concrete targets was based on the measured EM properties of concrete (Rhim, 1995; Rhim and Buyukozturk, 1998).

The constitutive relations describe the relationship between the EM fields in a medium defined by its EM properties. In general, the constitutive relations for a medium depend on its detailed physical structure, which may further depend on direction, temperature, frequency or other parameters (Staelin et al., 1994). In this research, when characterizing the EM properties of concrete, it is assumed that its physical structure is homogenous and isotropic, and the errors caused by these assumptions are neglected. Concrete is treated as a polarizable (dielectric), dispersive (frequency dependent), and lossy (conducting) medium and focus is placed on the effects of these properties in microwave scattering and imaging.

The constitutive relations to the Maxwell's equations characterize a homogenous and isotropic medium by its complex permittivity ϵ (farads/m) and complex permeability μ (henries/m) as follows (Staelin et al, 1994):

$$\vec{D} = \epsilon \vec{E} \quad (1)$$

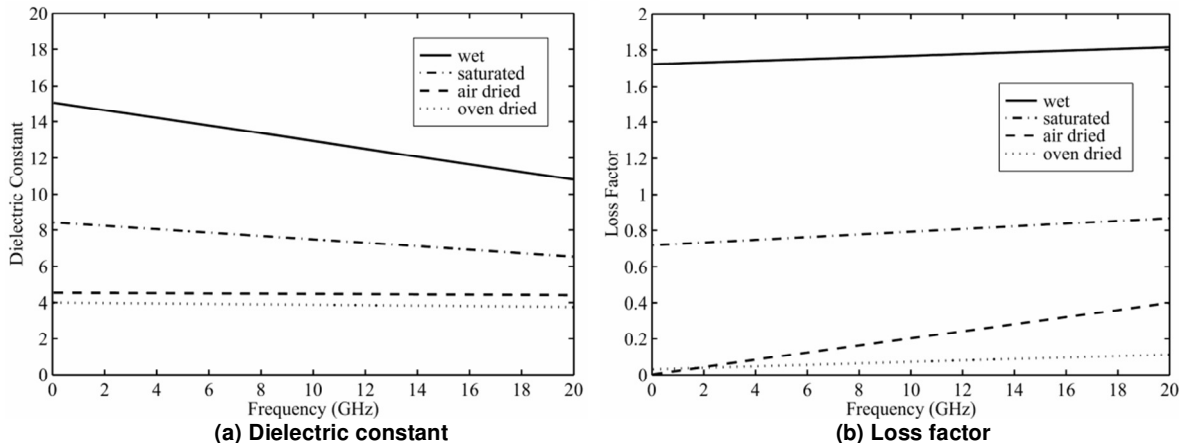


Figure 2. Measured EM properties of concrete between 0.1 to 20 GHz.

$$\vec{B} = \mu \vec{H} \quad (2)$$

where \vec{D} is electric flux density (Coulombs/m²), \vec{E} is electric field intensity (V/m), \vec{B} is magnetic flux density (webers/m²), and \vec{H} is magnetic field intensity (amperes/m). Theoretically, both the permittivity and permeability must be determined to characterize a homogenous and isotropic dielectric material. However, most common dielectric materials including concrete are nonmagnetic, meaning that the permeability μ is very close to the free space permeability μ_0 ($4\pi \times 10^{-7}$ Henry/m). Therefore, determination of its complex permittivity is sufficient to characterize a concrete medium.

Dielectric constant and loss factor

The complex permittivity, ϵ , defined in Equation 1 is often written in an explicit form as:

$$\epsilon = \epsilon' - j\epsilon'' \quad (3)$$

where ϵ' and ϵ'' are the real and imaginary parts of the complex permittivity, respectively. Dividing both sides of Equation 3 by the free space permittivity ϵ_0 (8.854×10^{-12} Farad/m) which is a real quantity, the complex permittivity of concrete can be expressed in a dimensionless form:

$$\epsilon_r = \epsilon_r' - j\epsilon_r'' \quad (4)$$

where the subscript r means relative to the free space

permittivity. The real and imaginary parts of the relative permittivity are referred to as the dielectric constant and the loss factor, respectively. The dielectric constant provides a physical indication of how polarizable a medium is, or alternatively, how much energy is stored in the medium when subjected to an electric field, while the loss factor is a measure of how lossy or dissipative a medium is to an external electric field.

The dielectric constant and loss factor, classified as the measured EM parameters are shown in Figure 2 for concrete for a frequency range from 0.1 to 20 GHz. It can be seen from Figure 2 that both the dielectric constant and loss factor of concrete increases dramatically with the increasing level of moisture (Figure 2a). This increase can be explained by the very high dielectric constant of water which varies somewhat linearly between eighty and forty in the frequency range from 0 to 20 GHz. A second important observation from Figure 2a is the frequency dependency of the dielectric constant for the same moisture level. It appears that the dielectric constant of concrete is not frequency dependent in dry condition; therefore no dispersion takes place in dry concrete. With the increasing moisture level, however, change of the dielectric constant with frequency becomes significant and concrete becomes dispersive. The slope of the change with frequency depends on the moisture level, and thus, is indicative of the moisture condition of concrete.

The measured values of the loss factor for concrete shown in Figure 2b are illustrative of the potential and a major limitation of microwave NDT of concrete. It shows that the loss of energy in dry concrete is not very significant up to relatively high frequencies, providing a reason to be optimistic about the applicability and success of the technique. However, it also draws attention to the problems due to moisture in terms of significant energy loss. The loss factor of concrete in saturated and wet conditions is significantly higher than in air and open

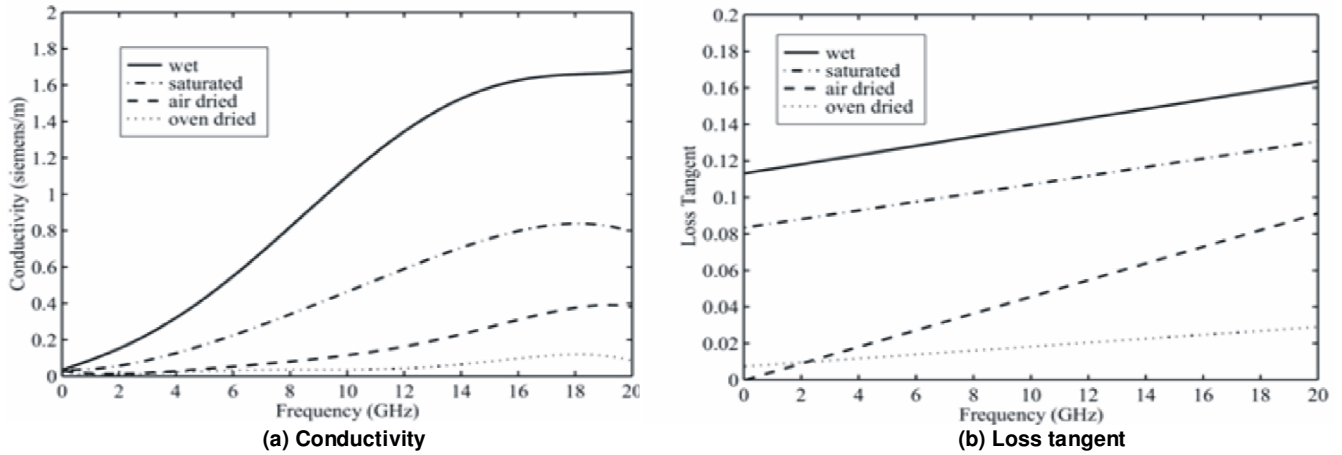


Figure 3. Derived EM properties of concrete between 0.1 to 20 GHz.

oven dry conditions. Change of the loss factor with frequency seems to occur more in air dried condition than at other moisture levels at which the increase is not significant.

Conductivity and loss tangent

The conductivity and loss tangent for concrete classified as the derived EM properties can be obtained from the dielectric constant and loss factor. The expression for conductivity, σ , is given by:

$$\sigma = \epsilon'' \omega \tag{5}$$

where ω is the angular frequency of the wave. The ratio between the imaginary and real parts of the complex permittivity is called the loss tangent, $\tan \delta$, of the medium which is a measure of how successfully the medium conducts in a dimensionless form:

$$\tan \delta = \frac{\epsilon''}{\epsilon'} = \frac{\sigma}{\omega \epsilon'} \tag{6}$$

Mathematically, a medium is called a good conductor if $\tan \delta \gg 1$ and a good insulator if the reverse is true.

The calculated values of conductivity and loss tangent for concrete are shown in Figures 3a and b, respectively. It appears from the figures that both parameters are sensitive to the moisture level and are frequency dependent. Conductivity of concrete at low frequency range is not significant for all moisture levels. With increasing frequency, effect of moisture becomes significant and conductivity of saturated and wet concrete shows a sharp increase. Conductivity of oven dried concrete stays close to zero over the entire measurement

frequency range while air dried concrete shows a slight increase with increasing frequency. Loss tangent of concrete is very similar in form to the loss factor shown in Figure 2b except that its frequency dependency is increased due to the division with the dielectric constant.

SIMULATION OF EM WAVE PROPAGATION AND SCATTERING

Simulation of the interaction of EM waves with a target that has known geometric and material properties is called the forward problem. A numerical simulation scheme called the finite difference-time domain (FD-TD) technique was implemented in 2-D to solve the forward problem (Lee, 1990; Li et al., 1992; Li, 1995). FD-TD technique involves numerical solution of the Maxwell's time dependent curl equations, which can be written in differential form for an isotropic, homogenous, dielectric and nonmagnetic material as:

$$\nabla \times \vec{E}(\vec{r}, t) = \frac{\partial \vec{D}(\vec{r}, t)}{\partial t} \tag{7}$$

$$\nabla \times \vec{H}(\vec{r}, t) = -\frac{\partial \vec{D}(\vec{r}, t)}{\partial t} + \sigma \vec{E}(\vec{r}, t) \tag{8}$$

The constitutive relations given by Equations 1 and 2 provide the additional relationships needed between field quantities to obtain a solution. Incorporating the EM properties of the target and applying the appropriate initial and boundary conditions that satisfy Maxwell's divergence equations (Staelin et al., 1994), a unique solution of the forward problem can be obtained using Maxwell's curl equations for a given excitation source.

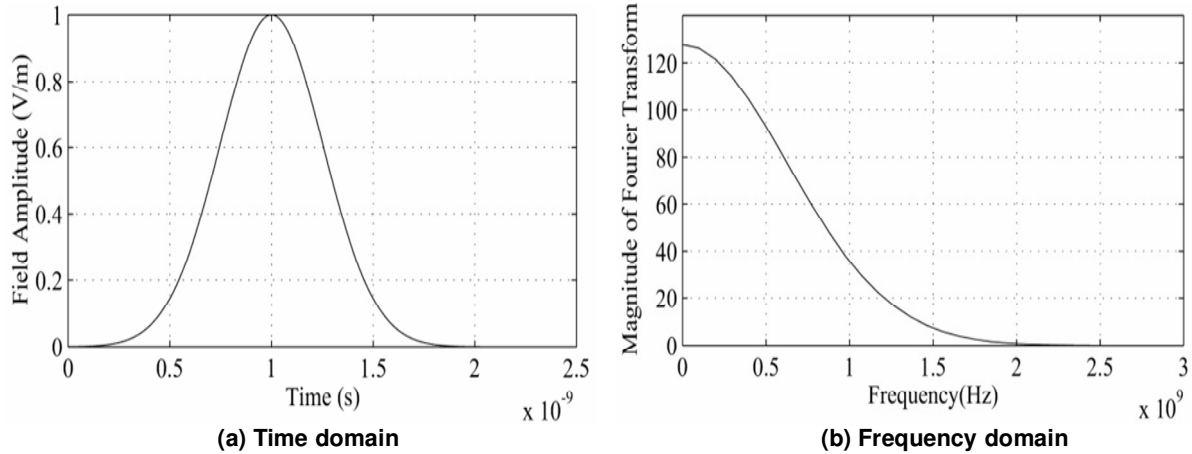


Figure 4. The Gaussian pulse excitation in time and frequency domain.

In the FD-TD technique, Maxwell's curl equations are discretized in time and space using center differences and the electric and magnetic fields are interlaced on a spatial grid. Generally, a rectangular grid is used due to its simplicity and ease of implementation. The fields are initially set to zero everywhere within the computational domain to satisfy Maxwell's divergence equations. Boundary conditions are enforced at the outer boundary of the computational domain as well as at all dielectric and conducting interfaces. These boundary conditions enforce continuity of the electric and magnetic fields at the interfaces between dielectric materials, and vanishing of the tangential electric field at the surface of perfect electric conductors such as the rebar in concrete. The fields are calculated everywhere in the computational domain in a leap-frog manner as a function of time, that is, first the electric fields are calculated, then the magnetic fields are calculated and the sequence is repeated at each time step. The grid spacing is required to be at most one tenth of the shortest wavelength of interest to ensure accuracy and the time step is determined by the Courant stability criterion. To simulate the unbounded space at the outer boundary of the computational domain, an approximate absorbing boundary condition is applied at the boundaries. Given the excitation source, which can be a plane wave or a point source, scattering of waves from one or more objects defined in the computation domain are found by marching in time.

Excitation source

A Gaussian pulse plane wave excitation was used as the incident field in the simulations. The advantage of using a Gaussian pulse is the ability to perform multi-frequency experiments simultaneously in one time domain simulation. The Gaussian pulse plane wave has the form:

$$\Phi_i(t) = e^{-2(t-t_0)^2/T^2} \quad (9)$$

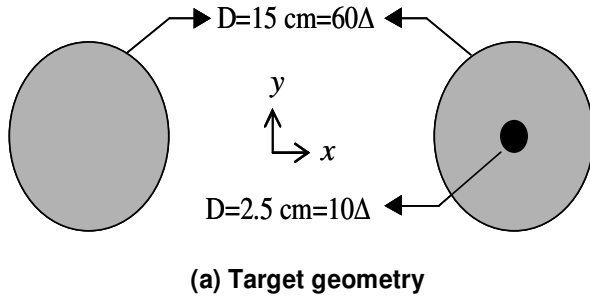
where $\Phi_i(t)$ (V/m) is the electric field amplitude of the incident wave, t is time, t_0 is the time delay, and T is the pulse width. The Gaussian pulse used in the simulations is shown in Figure 4 in both time and frequency domains. A pulse width $T = 0.5$ (ns) was chosen for the excitation source which corresponds to a maximum frequency of 1.5 GHz as shown in Figure 4b. This frequency range is chosen for the reason that it is representative of the currently used frequency range in Civil Engineering NDT applications. A narrower pulse can be used to increase the frequency content of the incident field and the information content of the scattered fields.

Grid size and time increment

The computational domain grid size and the time increment were calculated based on the knowledge of EM properties and the source excitation according to accuracy and stability criteria (Lee, 1990; Li et al., 1992; Li, 1995). For accuracy of the simulation, the grid size must be chosen at most one tenth of the smallest wavelength or the minimum scatterer dimension. The smallest wavelength was calculated using the maximum dielectric constant value for concrete (~ 15) from Figure 2a and the maximum frequency (~ 1.5 GHz) from Figure 4b as:

$$\lambda_{\min} = \frac{c}{f_{\max} \sqrt{\epsilon_{r\max}}} = \frac{3 \times 10^8}{1.5 \times 10^9 \sqrt{15}} = 0.05 \text{ (m)} \quad (10)$$

Defining the grids square in shape ($\Delta x = \Delta y = \Delta$) and



(b) EM properties

	Dry	Saturated
Dielectric c.	4	8
Conductivity	0	0.1

Figure 5. Geometry and EM properties of the targets.

setting their size conservatively to one twentieth of the minimum wavelength, the grid dimension was determined as $\Delta=2.5$ mm. Once the grid size was known, the time increment was calculated according to the Courant stability criterion as:

$$\Delta t \leq \frac{\Delta}{1.2c\sqrt{2}} = \frac{0.00254}{1.2(3 \times 10^8)\sqrt{2}} = 4.989 \times 10^{-2} \sim 0.005 \text{ ns} \quad (11)$$

where the constant 1.2 was introduced as a safety factor.

Geometry and electromagnetic (EM) properties of concrete targets

The concrete targets were modeled as cylindrical concrete specimens with and without a rebar at the center, assumed to be infinite in the z direction, allowing circular models in 2-D plane. The diameter of the concrete cylinder and the rebar were chosen as 15 and 2.5 cm which correspond to 60Δ and 10Δ , respectively. The geometry and dimensions of the targets are shown in Figure 5a. For each concrete model, a consistent set of EM properties were used and correspond to dry and saturated moisture conditions obtained from Figures 2a and 3a, respectively. The dielectric constant and conductivity values used to model these moisture conditions are shown in Figure 5b.

Size of the computational domain and the measurement lines

The factors considered in defining the size of the computational domain are the size of the scatterers and their distance to the boundaries of the computational domain. The absorbing boundaries due to their approximate nature may cause some reflections from the boundaries. Thus the scatterers must be placed away from the boundaries to ensure the accuracy of the simulation. Furthermore, the length of the measurement

line is an important factor in imaging since the information content of the measured data increases with increasing lengths of the measurement line. On the other hand, as the size of the computational domain increases, the computation time increases significantly since the fields are computed over the entire computational domain at each time step. Considering these factors, the size of the computational domain was defined as 600×300 in the x and y axes, respectively and the origin is placed at the center. The size in x direction was defined larger since the measurement lines are placed parallel to the x-axis, at $y = \pm 50 \Delta$ to measure both the reflected and transmitted waves. The length of the measurement line was chosen as 512Δ (-256Δ to 256Δ). Figure 6 shows the size of the computational domain, concrete scatterer and measurement lines in meters.

Finite difference-time domain (FD-TD) simulation results

A total of four simulations are presented in this paper for two models and two moisture levels as described in the previous sections. The concrete targets were illuminated by the Gaussian pulse plane wave from -y direction and only the scattered fields (subtracting the incident field) were measured at the measurement lines above and below the scatterer (Figure 6) in reflection and transmission modes, respectively. Each simulation was performed for two thousand time steps (~ 10 ns). The results of the simulations are shown in Figures 7 and 8 between 2.5 to 7.5 ns. It is seen from the figures that the transmitted and reflected fields measured over a line form hyperbolic arcs as expected. The amplitude of the reflection from the concrete surface given by the upper dark hyperbolic arcs increases with increasing moisture level. On the contrary, the amplitude of the back surface reflection shown by the lower dark hyperbolic arcs, decreases with increasing moisture due to excessive attenuation of EM waves in moist concrete. The presence of rebars is clearly indicated by two additional arcs for dry concrete. With increasing moisture, however, reflections from the rebar decrease significantly due to attenuation.

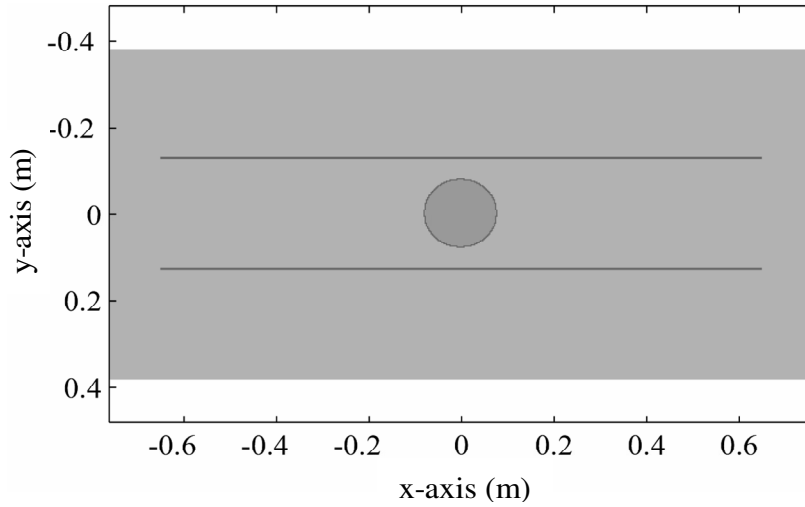


Figure 6. The computational domain, concrete scatterer and measurement lines.

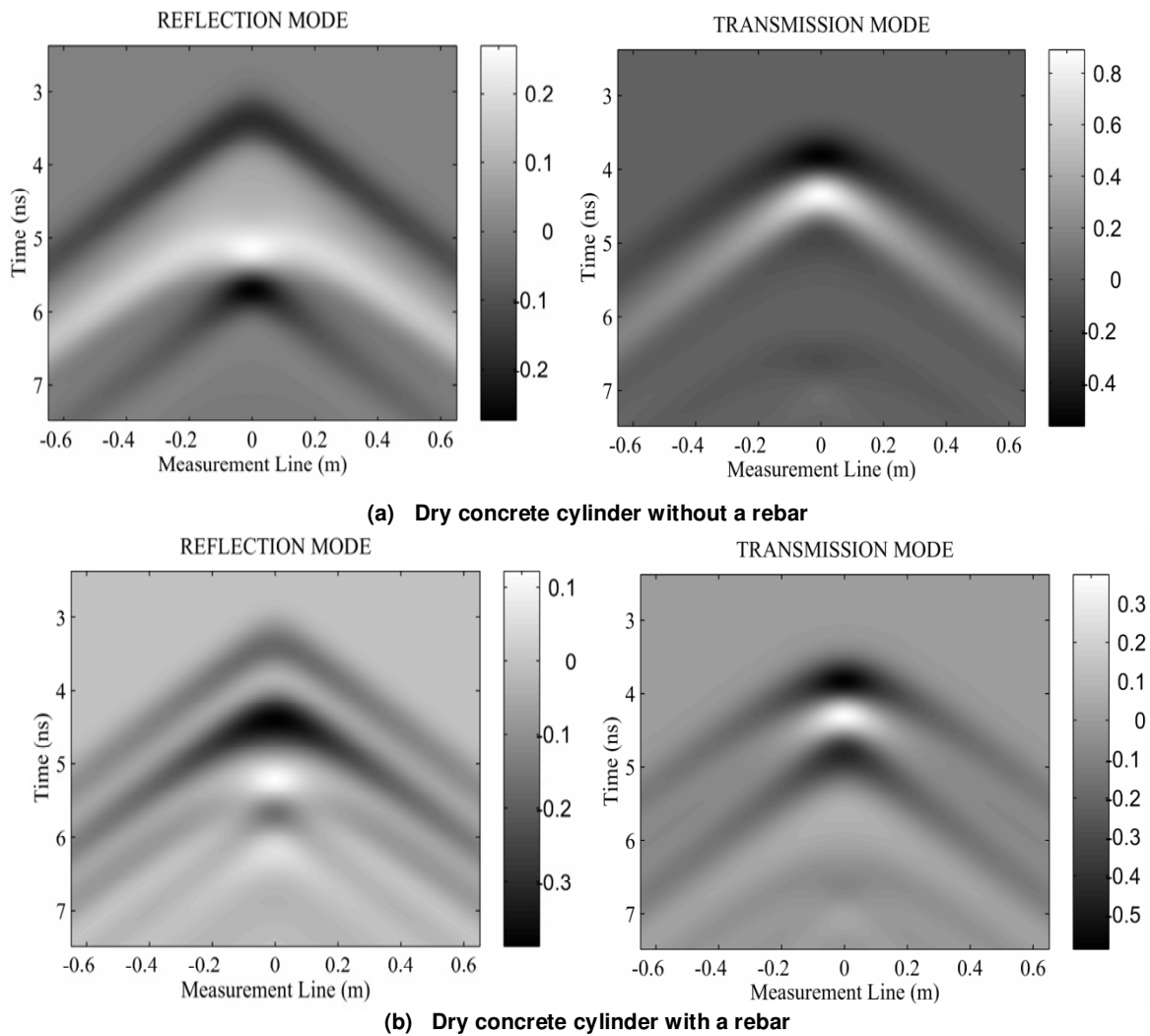


Figure 7. Scattered fields by the dry concrete cylinders with and without a rebar.

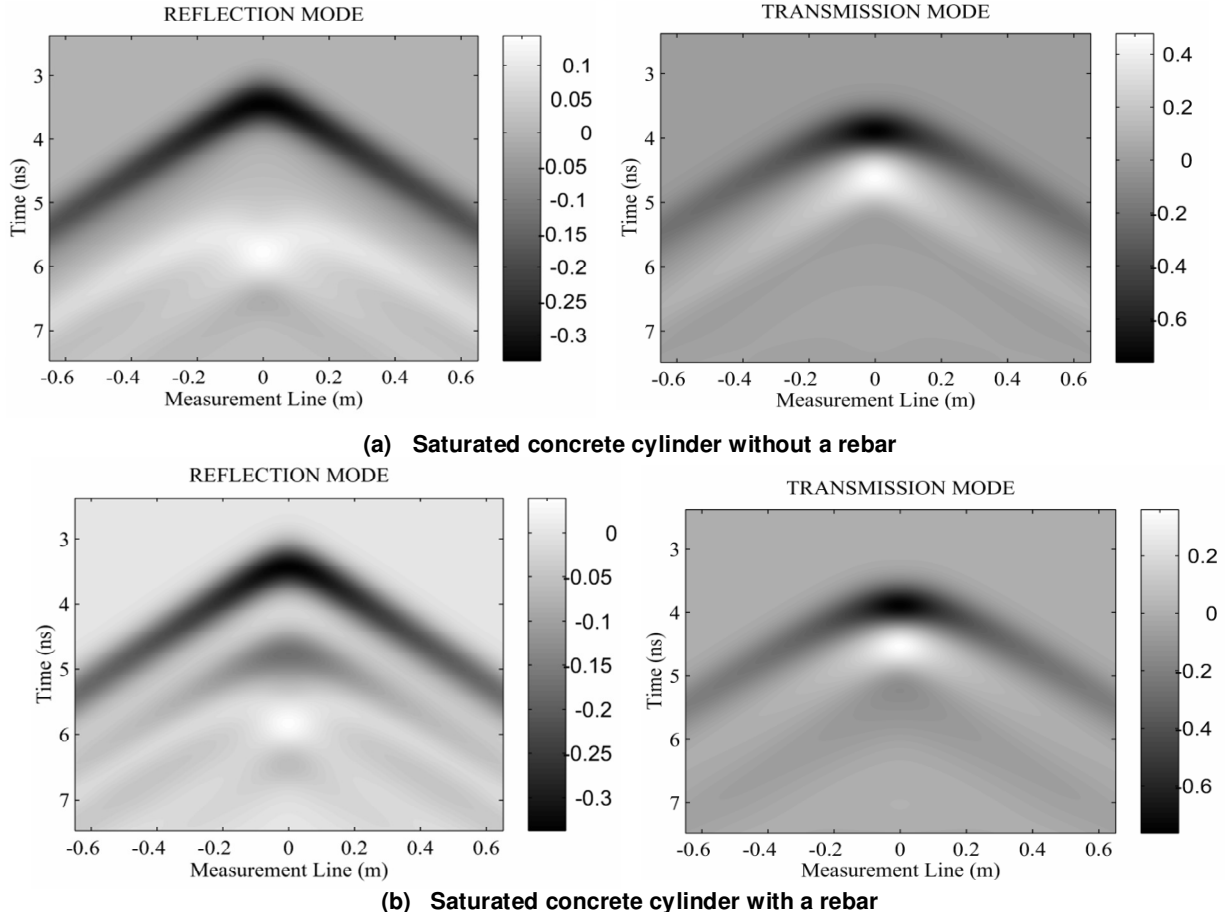


Figure 8. Scattered fields by the saturated concrete cylinders with and without a rebar.

IMAGE RECONSTRUCTION USING BACKPROPAGATION ALGORITHM

The backpropagation algorithm is a solution to the inverse source problem that attempts to determine the source (target) from its radiated fields. It is based on the inhomogeneous scalar wave (Helmholtz) equation and Huygen's secondary sources principle linearized by weak scatterer approximations (Herman et al., 1987; Boerner, 1983). The algorithm involves backpropagation of the scattered fields measured along a measurement line (planar surface in 3-D) towards the scatterer at incremental depths to obtain an image. For the case of multi-frequency experiments, the procedure can be repeated for each temporal frequency (or wavelength) and superimposed since the procedure is linear. The final image is obtained by taking the inverse Fourier transforms of the superimposed fields at each depth. This procedure is illustrated in Figure 9. In a microwave scattering experiment, the measured data can be either in time or frequency domain depending on the equipment used. Assuming the field at the measurement line is recorded in the time domain, the algorithm can be described step by step as follows (Herman et al., 1987):

- 1) Take the Fourier transform of the field recorded along the line $\Phi_s(x, y = 0, t)$ with respect to time t to obtain $\Phi_s(x, y = 0, \omega)$.
- 2) Take the spatial Fourier transform of $\Phi_s(x, y = 0, \omega)$ with respect to x to obtain $\hat{\Phi}_s(K_x, y = 0, \omega)$.
- 3) To obtain the field distribution at $(y = -d_i)$, back propagate the transformed field $\hat{\Phi}_s(K_x, y = 0, \omega)$ to this position for each ω using

$$\hat{\Phi}_s(K_x, y = -d_i) = \int_{\omega_{\min}}^{\omega_{\max}} \hat{\Phi}_s(K_x, y = 0, \omega) \hat{P}(K_x, y = -d, k_0) \Big|_{k_0 = \frac{c}{\omega}} d\omega \quad (11)$$

where, \hat{P} , the backward propagator, is given by

$$\hat{P}(K_x, y, k_0) = \begin{cases} e^{jy\sqrt{k_0^2 - K_x^2}} & K_x < k_0 \\ 0 & K_x \geq k_0 \end{cases} \quad (12)$$

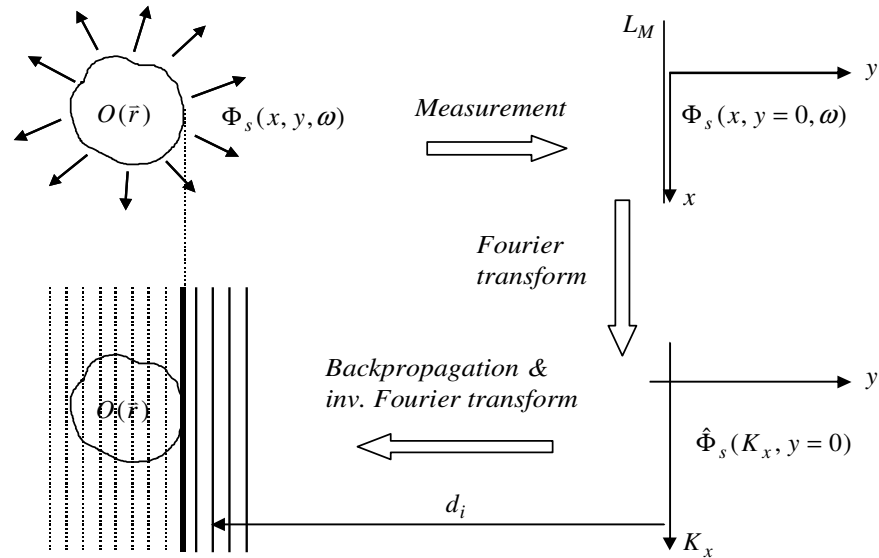


Figure 9. Image reconstruction using backpropagation of wave fields.

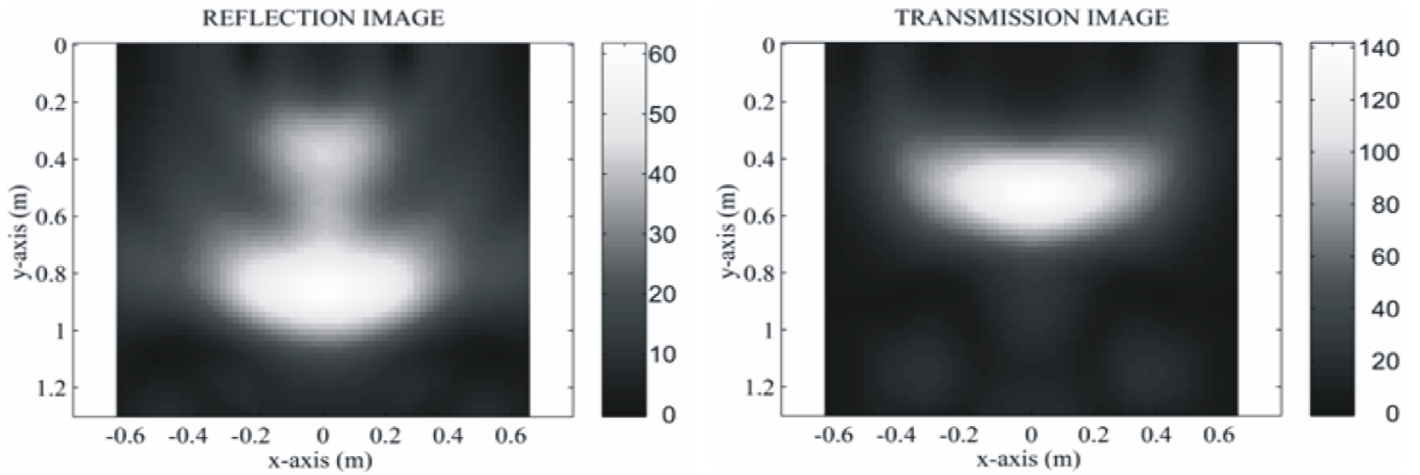
- 4) Take the inverse Fourier transform of $\hat{\Phi}_s(K_x, y = -d_i)$ with respect to K_x to find the field distribution $\Phi_s(x, y = -d_i)$ at this new position.
- 5) Repeat 3 and 4 at incremental depths to form a 2-D image of the scatterer.

Images reconstructed from the scattered fields shown in Figures 7 and 8 by implementing the previously described backpropagation algorithm are shown in Figures 10 and 11, respectively. As shown in the figures, the backpropagation algorithm essentially collapses the hyperbolic arcs that appear in the images of the scattered data shown in Figures 7 and 8. A comparison of the images shows that transmission mode experiments generally result in more accurate images. Except for the reflection image of the dry concrete cylinder with a rebar in Figure 10b, all images show the concrete cylinder. The size of the cylinder, however, generally appears larger than the actual model. The presence of the rebar resulted in a distorted image in Figure 10b, which was expected since the rebar severely violates the linearizing (weak scatterer) approximation used in the algorithm's formulation. The distortion due to rebar disappears in saturated condition due to attenuation. All the transmission images appear to be relatively insensitive to the presence of a rebar in concrete which is most probably due to the large pulse width of the incident wave resulting in low range and cross-range resolution.

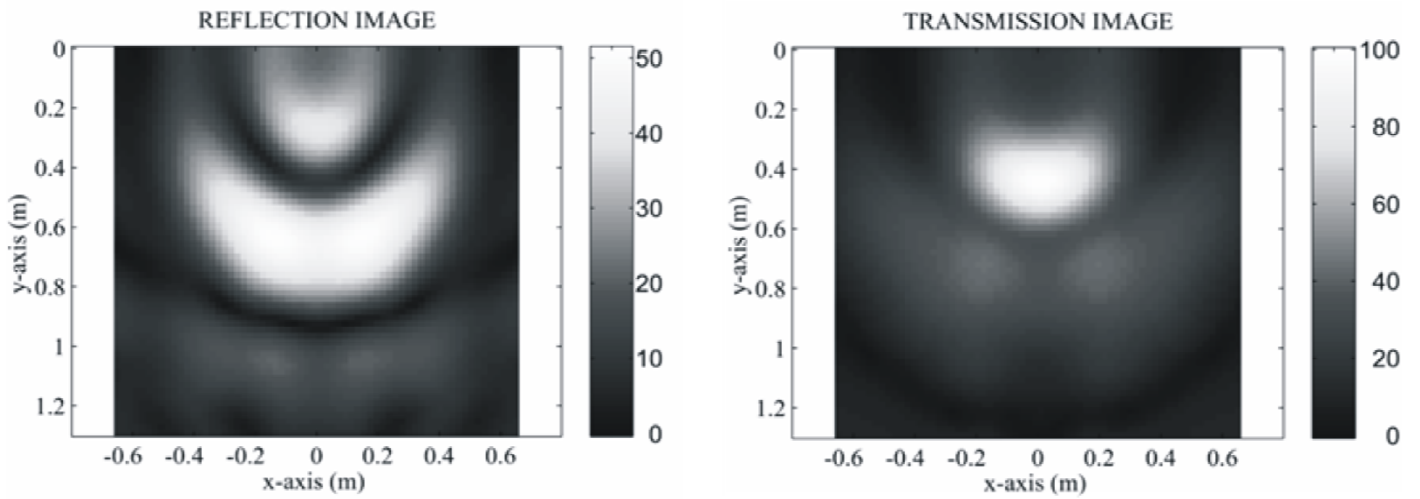
Conclusions

Based on the results of imaging applications, the following conclusions were drawn:

- 1) Microwave imaging is a promising method with high potential benefits in non-contact NDT of concrete structures provided that its capabilities and limitations are well understood.
- 2) The imaging applications performed on concrete cylinders in this research were moderately successful in reconstructing the geometry of the concrete target. The reconstructed images are easier to interpret than the raw scattered data, although the size of the reconstructed image appears generally larger than the target size. In addition, presence of reinforcement in concrete may result in distortions in the reconstructed image. These limitations can be attributed to the limitations of the algorithm such as the linearizing approximations in its formulation, partial processing in the Fourier domain, and the frequency content of the source excitation.
- 3) Material properties of concrete have significant effects in forward and inverse scattering of microwaves. Attenuation of waves takes place in concrete at high moisture levels and results in weak reflections from back surface of the concrete target and the rebar. Images of concrete cylinders with and without a rebar show no significant difference at saturated condition; which implies that the reflections from rebar vanish before they reach the measurement line.
- 4) The frequency content of the excitation pulse used in the simulations is representative of the frequency range currently used in Civil Engineering NDT applications. The imaging results show that the frequency content of the incident field must be increased in order to improve the resolution.
- 5) The backpropagation algorithm used for imaging essentially collapses the hyperbolic arcs that appear in the images of the scattered fields. The reconstructed images are easier to interpret compared to the scattered

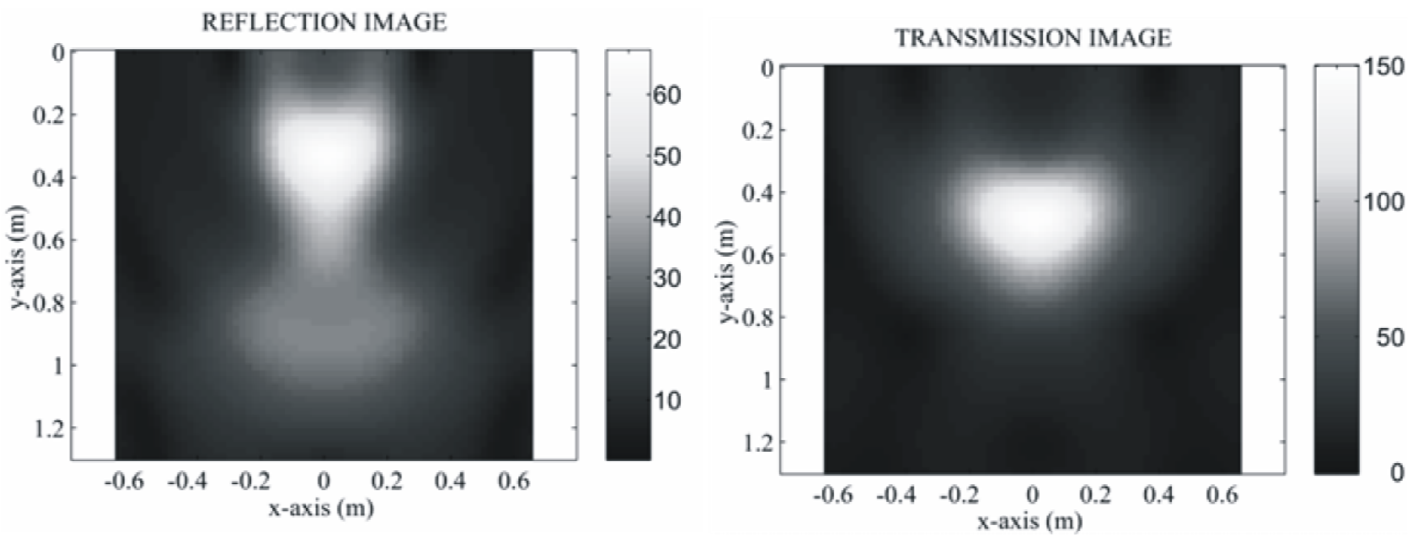


(a) Dry concrete cylinder without a rebar



(b) Dry concrete cylinder with a rebar

Figure 10. Reconstructed images of dry concrete cylinders with and without a rebar.



(a) Saturated concrete cylinder without a rebar

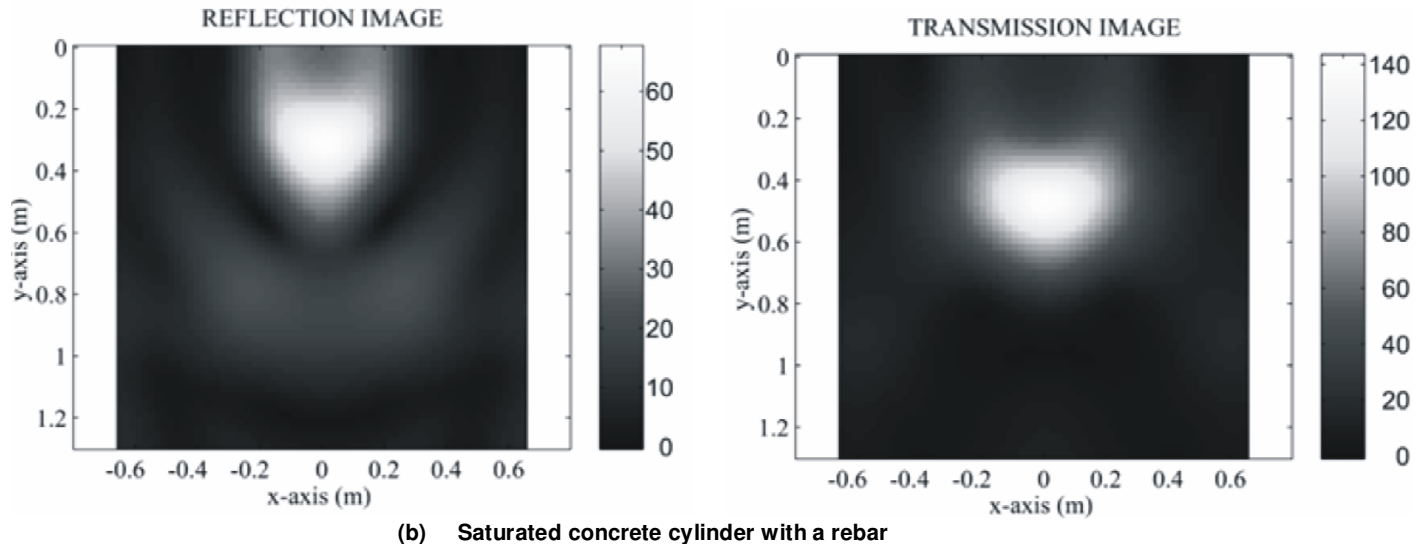


Figure 11. Reconstructed images of saturated concrete cylinders with and without a rebar.

data, but their advantage on their own in terms of the quality of information they provide is debatable. Combined evaluation of the scattered data and reconstructed images, however, is likely to improve the efficiency and accuracy of NDT.

REFERENCES

- Bertero M, Pike ER (1992). Inverse problems in scattering and imaging. NATO Advanced Research Workshop, Cape Cod, USA, p. 550.
- Boerner WM (1983). Inverse methods in electromagnetic imaging. NATO ASI Series, D. Reidel Publishing Company, Dordrecht. C-143.
- Buyukozturk O (1998). Imaging of concrete structures. *NDT&E Int.*, 31(4): 233-243.
- Buyukozturk O, Yu TY (2009). Far-field radar NDT technique for detecting GFRP debonding from concrete. *Constr. Build. Mater.*, 23(4): 1678-1689.
- Cartz L (1995). *Nondestructive testing*. ASM International, OH, p. 229.
- Herman GT, Tuy HK, Langenberg KJ, Sabatier PC (1987). *Basic methods of tomography and inverse problems*. Adam Hilger, Bristol, p. 680.
- Kak AC, Slaney M (1988). *Principles of computerized tomographic imaging*. IEEE Press, New York, p. 327.
- Lee CF (1990). Finite difference method for electromagnetic scattering problems. Ph.D. Thesis, Depart. Elect. Eng. Comput. Sci. MIT, Cambridge, MA, p. 192.
- Li K (1995). Finite difference time domain analysis of electromagnetic interference and radiation problems. Ph.D. Thesis, Electrical Engineering And Computer Science Department, MIT, Cambridge, MA, p. 264.
- Li K, Tassoudji MA, Shin RT, Kong JA (1992). Simulation of electromagnetic radiation and scattering using a finite difference-time domain technique. *Comput. Appl. Eng. Educ.*, 1(1): 45-63.
- Rhim HC (1995). *Nondestructive evaluation of concrete using wideband microwave techniques*. Ph.D. Thesis, Department of Civil and Environmental Engineering, MIT, Cambridge, MA, p. 232.
- Rhim HC, Buyukozturk O (1998). Electromagnetic properties of concrete at microwave frequency range. *ACI Mater. J.*, 95(3): 262-271.
- Staelin DH, Morgenthaler AW, Kong JA (1994). *Electromagnetic waves*, Prentice Hall, Englewood Cliffs, New Jersey, p. 562.
- Yu TY, Buyukozturk O (2009). A far-field airborne radar NDT technique for detecting debonding in GFRP-retrofitted concrete structures. *NDT&E Int.*, 41(1): 10-24.